ELSEVIER

● *Original Contribution*

A FOUR-CRITERION SELECTION PROCEDURE FOR ATHEROSCLEROTIC PLAQUE ELASTICITY RECONSTRUCTION BASED ON *IN VIVO* CORONARY INTRAVASCULAR ULTRASOUND RADIAL STRAIN SEQUENCES

SIMON LE FLOC'H,* GUY CLOUTIER,†‡ YOSHIFUMI SAIJO,§ GÉRARD FINET,|| SAAMI K. YAZDANI,¶ FLAVIEN DELEAVAL,* GILLES RIOUFOL,|| RODERIC I. PETTIGREW,# and JACQUES OHAYON*,**

*Laboratory TIMC-IMAG/DyCTiM, UJF, CNRS UMR 5525, Grenoble, France; †Laboratory of Biorheology and Medical Ultrasonics, University of Montreal Hospital Research Center (CRCHUM), Montréal, Québec, Canada; ‡Department of Radiology, Radio-Oncology and Nuclear Medicine, and Institute of Biomedical Engineering, University of Montreal, Montréal, Québec, Canada; §Department of Biomedical Engineering, Tohoku University, Sendai, Japan; ||Department of Hemodynamics and Interventional Cardiology, Hospices Civiles de Lyon and Claude Bernard University Lyon 1, INSERM Unit 886, Lyon, France; ¶CVPath Institute, Gaithesburg, MD, USA; #Laboratory of Integrative Cardiovascular Imaging Science, NIDDK, NIH, Bethesda, MD, USA; and **University of Savoie, Polytech Annecy-Chambéry, Le Bourget du Lac, France

Abstract—Plaque elasticity (*i.e.*, modulogram) and morphology are good predictors of plaque vulnerability. Recently, our group developed an intravascular ultrasound (IVUS) elasticity reconstruction method which was successfully implemented *in vitro* using vessel phantoms. *In vivo* IVUS modulography, however, remains a major challenge as the motion of the heart prevents accurate strain field estimation. We therefore designed a technique to extract accurate strain fields and modulograms from recorded IVUS sequences. We identified a set of four criteria based on tissue overlapping, RF-correlation coefficient between two successive frames, performance of the elasticity reconstruction method to recover the measured radial strain, and reproducibility of the computed modulograms over the cardiac cycle. This four-criterion selection procedure (4-CSP) was successfully tested on IVUS sequences obtained in twelve patients referred for a directional coronary atherectomy intervention. This study demonstrates the potential of the IVUS modulography technique based on the proposed 4-CSP to detect vulnerable plaques *in vivo*. (E-mail: Jacques.Ohayon@imag.fr)   © 2012 World Federation for Ultrasound in Medicine & Biology.

INTRODUCTION

Atherosclerotic plaque rupture is the major cause of acute coronary syndrome, myocardial infarction and stroke in the western world (Virmani et al. 2000). The thin-cap fibroatheroma (TCFA) is the precursor lesion that once ruptured, may lead to the formation of a thrombus causing an acute syndrome and possibly death (Virmani et al. 2006). Typically, an unstable vulnerable coronary plaque (VP) has a large extracellular necrotic core thickness, a fibrous cap thickness less than 65 μm and activated macrophages (Virmani et al. 2000; Ohayon et al. 2008). Cellular mechanisms associated with plaque instability include inflammation, reduced collagen synthesis, local expression of collagenase and smooth muscle cell apoptosis (Falk et al. 1995). Such biologic processes alter mechanical properties of the plaque surface (Arroyo and Lee 1999).

Coronary VPs can be detected clinically by various intravascular techniques, including ultrasound (IVUS) (Rioufol et al. 2002; Carlier and Tanaka 2006), optical coherence tomography (OCT) (Jang et al. 2002; Tearney et al. 2008) and magnetic resonance imaging (IV-MRI) (Larose et al. 2005; Briley-Saebo et al. 2007). Predicting coronary plaque rupture, on the other hand, is still imprecise, as imaging features of plaque morphology and composition are insufficient predictors of risk (Loree et al. 1992; Ohayon et al. 2008). Prediction of rupture also requires knowledge of the plaque elasticity (Ohayon et al. 2001; Finet et al. 2004), thus, numerically estimating the peak stress amplitude of the fibrous cap, which appears to be a good biomechanical predictor of plaque rupture (Loree et al. 1992; Ohayon et al. 2008).

Therefore, the plaque elasticity reconstruction (*i.e.*, modulogram) is an essential step for a reliable computation of intraplaque stresses.

Computation of such elasticity maps, based on the estimation of the intraplaque strain field (*i.e.*, elastogram) obtained from various ultrasound-based techniques (Wan et al. 2001; de Korte et al. 2002; Kim et al. 2004; Maurice et al. 2007; Zhang et al. 2010; Hu et al. 2011) and OCT (Chan 2004; Rogowska et al. 2004; van Soest et al. 2007) remains a difficult task that has been tackled by a rather large diversity of approaches (Vorp et al. 1995; Vonesh et al. 1997; Beattie et al. 1998; Kim et al. 2004; Fehrenbach et al. 2006; Baldewsing et al. 2008; Cimrman and Rohan 2010; Pazos et al. 2010; Franquet et al. 2011; Doyley 2012). Our group recently proposed a robust IVUS elasticity modulus approach for plaque imaging that combined a dynamic watershed segmentation (DWS) method with an optimization procedure (Le Floc'h et al. 2009). This Young's modulus reconstruction approach "iMOD" was successfully tested *in vitro* on polyvinyl alcohol cryogel vessel phantoms with controlled intraparietal stiffness inclusions (Le Floc'h et al. 2010).

Plaque elasticity reconstruction models based on IVUS strain sequences in patients, however, are difficult due to motions created by the contraction and relaxation of the myocardium and the pulsatile nature of the coronary flow, preventing optimum strain field measurements and precise tracking of a same vessel cross-section during the whole cardiac cycle. Although original local sine-wave approach (Arts et al. 2010), spatial priors techniques (Richards et al. 2011) or more appropriate regularization technique (Doyley 2012) could potentially overcome these hurdles, an alternative strategy would be to "precondition" the algorithm by selecting reliable input plaque strain and displacement fields, which is the main goal of the current study. We, therefore, designed a technique to extract accurate strain fields and modulograms from recorded IVUS sequences. We identified a set of four criteria based on (1) tissue overlapping, (2) RF-correlation coefficient between two successive frames, (3) performance of the elasticity reconstruction method to recover the measured radial strain, and (4) reproducibility of the computed set of modulograms over the cardiac cycle. This four-criterion selection procedure was successfully tested on IVUS sequences obtained in 12 patients referred for a directional coronary atherectomy (DCA) intervention.

METHODS

IVUS image analysis and plaque strain reconstruction

The first step of the IVUS data preprocessing consisted of segmenting IVUS images to detect vessel boundaries. The segmentation algorithm to detect the lumen and adventitia boundaries was based on a fast-marching model combining region and contour information (Roy Cardinal et al. 2006). Contours were validated by a cardiologist before the next processing step. The artery wall (area between the detected lumen and adventitia boundary) defined the region-of-interest (ROI) and was used for image registration before the radial strain estimation. The second step consisted of a rigid motion compensation to remove the rotation observed between consecutive images. Each IVUS frame made of 256 radial lines in polar coordinates was unwrapped to obtain a matrix where rows correspond to propagation depths and columns to angles. A lateral translation in this representation, thus, corresponded to a rotation centered on the middle of the catheter in the Cartesian system. The first 256 columns were selected as the initial image of the sequence. The second image was searched by lateral 2-D correlations of regions-of-interest (ROIs) and the rotation artifact was determined as the lateral shift with maximum correlation. Next, the new image compensated for rotation served as the initial image to align the third one and so on. A complete sequence was reconstructed with all images compensated for rotation. Finally, the radial strain was computed using the Lagrangian speckle model estimator (LSME) (Maurice et al. 2004). The first step of this algorithm consisted of a local rigid registration on overlapping sub-windows (measurement windows [MWs]) within the ROI that allowed compensating for potential residual translation movement using a 2-D cross-correlation analysis. Then, for each MW, displacement field and RF-correlation coefficient were computed. Notice that the LSME algorithm was formulated as a nonlinear minimization problem based on the optical flow equations solved for each MW. This technique allows direct assessment of the spatial radial strain distribution (ε_{rr}^{LSME}) (Maurice et al. 2004).

Plaque elasticity reconstruction method

The theoretical framework of this method has been described earlier (Le Floc'h et al. 2009). Briefly, considering two successive frames (at time t_{j-1} and t_j) of the IVUS sequence, we applied the imaging modulography technique (iMOD), which involves three successive steps: (1) the computation of a pseudo-gradient elasticity map, (2) the DWS segmentation procedure that makes use of the previous step results to extract the inclusions' contours, and finally (3) the mathematical optimization procedure that provides the estimated Young's moduli of detected inclusions and surrounding tissue. The last step (3) relies on using the adjoint method to estimate the gradient of the root mean squared error (RMS_{error}) between the intraplaque measured ε_{rr}^{LSME} and computed ε_{rr}^{iMOD} radial strains:

$$RMS_{error}\left(t_j\right) = \frac{1}{n}\sqrt{\sum_{i=1}^{n}\left[\varepsilon_{rr}^{LSME}\left(t_j, x_i\right) - \varepsilon_{rr}^{iMOD}\left(t_j, x_i\right)\right]^2} \tag{1}$$

where n is the total number of nodes in the plaque mesh and x_i the position of the plaque node i. In this process, a Young's modulus set solution was found acceptable when the gradient-based optimization procedure reached either a tolerance termination value lower than 10^{-6} or a maximum number of iterations equal to 200. During the optimization procedure, local Young's moduli were constrained to remain positive and between 1 kPa and 10^4 kPa.

Four-criterion selection procedure used to extract plaque modulograms

For each patient's atherosclerotic lesion, approximately 30 displacement maps were reconstructed based on the IVUS sequence recorded during one second. We used four criteria to extract accurate displacement, strain and elasticity maps. The first criterion estimates the quality of the measured displacement field (displacement quality index Q_{displa}); the second criterion estimates the accuracy of the spatial distribution of the RF-correlation coefficient between two successive frames (tracking quality index Q_{track}); the third criterion estimates the propensity of the Young's modulus reconstruction method to recover the measured radial strain (strain quality index Q_{strain}) and finally, the last criterion estimates the reproducibility of resulting modulograms over the cardiac cycle (reproducibility quality index Q_{reprod}).

Displacement quality index (Q_{displa})

The displacement field resulting from the LSME process was used to detect sites with inaccurate measurements corresponding to regions with tissue overlap, which induces strain artifacts. An overlapping region was defined as a site where the regular polar mesh is strongly distorted so that an element overlaps its neighbouring elements. Such conditions are not physically admissible. The positions of the nodes of the elements in the deformed

configuration were obtained by using the displacement vector estimated at each node of the regular polar mesh

thanks to the LSME algorithm. Therefore, to select only frames with few tissue overlap sites, a global displacement quality index ($0\% \leq Q_{displa} \leq 100\%$) was defined at each time-frame t_j as:

$$Q_{displa}\left(t_j\right) = 100\left[\frac{1}{n}\sum_{i=1}^{n} q_{displa}\left(t_j, x_i\right)\right] \tag{2}$$

where q_{displa} is a local value associated to the position x_i and equal either to 0 or 1 whether an overlapping is observed or not, respectively. The parameter n is the total number of pixels representing the cross-section image of the pathologic artery. To minimize the effects of such inaccurate displacement sites on plaque elasticity reconstruction, only frames for which more than 60% of the plaque area was found without tissue overlaps (i.e., with local q_{displa} value equal to 1) were kept for our analysis (i.e., with $Q_{displa} \geq 60\%$).

Tracking quality index (Q_{track})

The tracking quality index results, obtained from the LSME process, highlight the robustness of the MW tracking method. This criterion Q_{track} was defined for each time-frame t_j as:

$$Q_{track}\left(t_j\right) = 100\left[\frac{1}{n}\sum_{i=1}^{n} q_{correl}\left(t_j, x_i\right)\right] \tag{3}$$

where q_{correl} is the local RF-correlation coefficient measured at position x_i ($0 \leq q_{correl} \leq 1$) (Maurice et al. 2004). The amplitude of the criterion Q_{track} varies from $0\% \leq Q_{track} \leq 100\%$; low values indicate that almost all MWs were poorly tracked due to the out-of-plane motion of either the catheter or the arterial wall. At the opposite, high values of Q_{track} point out accurate tracking of all MWs. Only frames for which Q_{track} exceeded 60% were kept for our analysis.

Strain quality index (Q_{strain})

To estimate the reliability of computed strain fields obtained with the iMOD algorithm, we defined for each time-frame t_j the following strain quality index:

$$Q_{strain}\left(t_j\right) = 100\left[1 - \left(\frac{\sum_{i=1}^{n}\left|\varepsilon_{rr}^{iMOD}\left(t_j, x_i\right) - \varepsilon_{rr}^{LSME}\left(t_j, x_i\right)\right|}{\sum_{i=1}^{n}\left|\varepsilon_{rr}^{LSME}\left(t_j, x_i\right)\right|}\right)^2\right] \tag{4}$$

where $0\% \leq Q_{strain} \leq 100\%$. A high value of Q_{strain} indicates a good match between the LSME-measured and

iMOD-estimated strain fields. Only frames for which Q_{strain} exceeded 60% were kept.

Reproducibility quality index of modulograms (Q_{reprod})

For a given IVUS sequence, only N* frames, for which all three quality indexes Q_{displa}, Q_{track} and Q_{strain} exceeded 60%, were kept. The reproducible quality index determines the similarity between modulograms. Such criterion rejects modulograms that deviate from a specific mean modulus elastogram. This specific mean elasticity map was computed by averaging the best combination of the extracted K reproducible modulograms ($2 \leq K \leq N*$). Since we are looking simultaneously for the best reproducible combination of K modulograms and the resulting specific mean modulogram, extensive simulations were performed. Thus, for each patient, $\sum_{K=2}^{N*} C_{N*}^{K}$ combinations of K modulograms were selected and $\sum_{K=2}^{N*} K\, C_{N*}^{K}$ reproducibility quality indexes Q_{reprod} were computed. This index, for a given jth modulogram ($1 \leq j \leq K$), was estimated by computing the relative change between its value at time t_j (*i.e.*, the spatial Young's modulus map $E(t_j, x_i)$) and the mean reference Young's modulus map $\tilde{E}_K(x_i)$ averaged over all K modulograms:

$$Q_{reprod}(t_j) = 100 \left[1 - \left(\frac{\sum_{i=1}^{n} |E(t_j, x_i) - \tilde{E}_K(x_i)|}{\sum_{i=1}^{n} \tilde{E}_K(x_i)} \right)^2 \right] \tag{5}$$

$$\text{with } \tilde{E}_K(x_i) = \frac{1}{K} \sum_{j=1}^{K} E(t_j, x_i) \tag{6}$$

The best set of K reproducible modulograms was defined as the combination with the higher Q_{reprod} mean value. From this best set, the final modulogram was chosen as the one with the higher Q_{strain} value. In situations where Q_{reprod} mean value remained less than 60% (*i.e.*, when the modulograms are not reproducible), the final modulogram was chosen to be the one with the higher Q_{strain} amplitude.

Validation of the four-criterion selection procedure

The elasticity reconstruction method was conducted by using a four-criterion selection procedure (4-CSP) in which the four criteria Q_{displa}, Q_{track}, Q_{strain} and Q_{reprod} were applied successively. However, to investigate the impact of each criterion, we selected modulograms by applying them individually on the whole database of 12 IVUS sequences of patients referred for DCA intervention.

Clinical data and histologic study on excised DCA lesions

Selected patients (including two no re-flow cases and one perforation case) gave their written informed consent before being recruited. The research protocol was approved by the Review Ethical Committee of Sendai University hospital. All 12 patients were scheduled to undergo a DCA intervention. Routine IVUS observations were performed and RF signals were acquired at the same moment. IVUS scans were conducted with a Galaxy II$^{®}$ echograph (Boston Scientific, Natick, MA, USA) equipped with 40 MHz mechanically rotating probes. One sequence of approximately 30 images was acquired for each patient with a fixed longitudinal position of the catheter within the maximum stenosis, at a frame rate of 30 images/s. Blood pressure increment between acquired RF images was assessed by assuming a linear variation between normal systemic diastolic and systolic phases.

The DCA procedure consisted in removing part of the atherosclerotic plaque with a catheter designed for radial lesion cutting and excision (Flexicut, Guidant Corporation, Santa Clara, CA, USA). The excised specimens were fixed in 10% formalin. The samples were then embedded in paraffin using standard protocols and 4 μm transversal slices were obtained using a microtome for histological staining with Elastica-Masson's thrichrome. Such staining gave information on plaque constituents only. Indeed, due to the DCA technique, only the excised "deteriorated" portions of the atherosclerotic plaques and not the intact excised lesions were collected making it impossible to correlate between the modulogram image and the plaque morphology. We, therefore, investigated only the atherosclerotic plaque composition by performing the histologic study.

The DCA procedure does not remove the whole lesion. A post DCA IVUS scan was performed for all patients. But unfortunately we were unable to identify the extracted part of the lesion by using this post DCA IVUS scan. After DCA procedure, the cross-section of the coronary (at the level of the treated lesion) becomes smaller (due to a global contraction process) making the superposition between the pre and post DCA IVUS images impossible. Therefore, we asked the cardiologist to roughly define on the pre DCA IVUS image the boundary of the lesion that was excised during the DCA procedure.

Image analysis of the histologic samples

Histologic stained samples were observed using a microscope, with images acquired concomitantly. Each image was then digitized and saved to a computer for postprocessing.
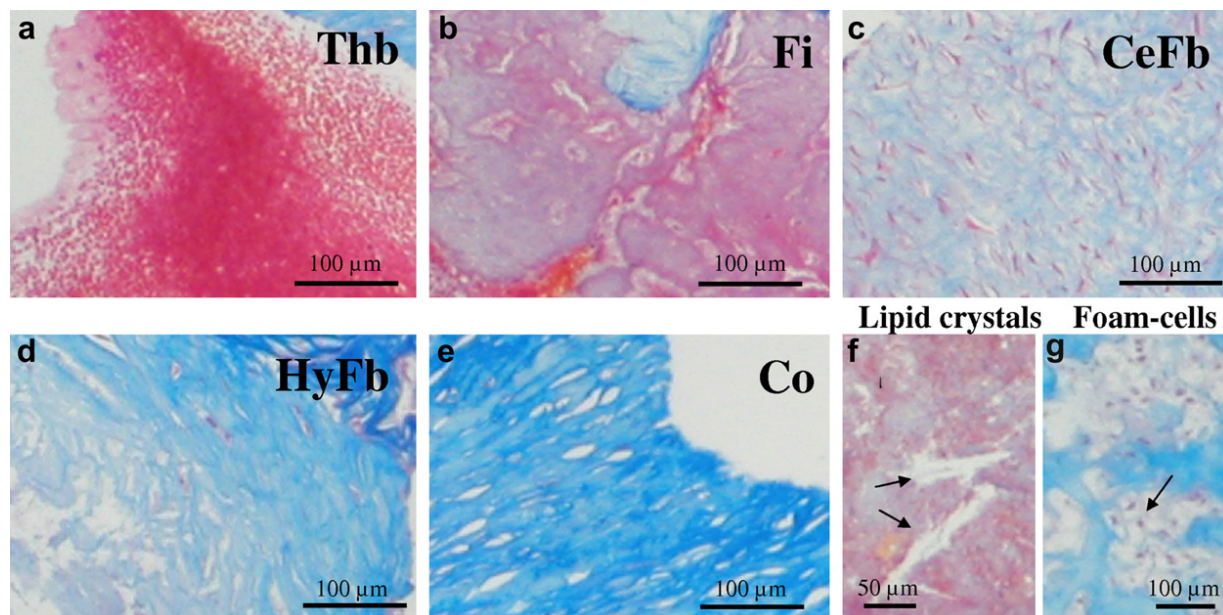
Fig. 1. Images showing morphologically distinguishable subtypes of atherosclerotic plaque constituents. (a) Thrombotic (Thb) region. (b) Fibrin (Fi) region. (c) Cellular fibrous (CeFb) region. (d) Hypocellular fibrous (HyFb) region. (e) Collagen (Co) region. (f) Lipid crystals (arrows). (g) Macrophage-derived foam-cells (arrow). See text for complete description.

Atherosclerotic plaque composition and characterization

The elastica-Masson's trichrome (EMT) staining was used to subdivide atherosclerotic excised lesions into seven distinct constituents (Fig. 1). The thrombotic (Thb) and the fibrin (Fi) regions consisted of high density of red blood cells and fibrin, respectively; the cellular fibrous (CeFb) region consisted of smooth muscle cells or other cells admixed with a low collagen content or elastic fiber; the hypocellular fibrous (HyFb) region contained extracellular connective tissue matrix with collagen and few cells; the collagen (Co) region was defined as site with high density of collagen fibers.

The intensity of the blue staining color reveals the amount of collagen content (strong blue indicates sites with high collagen content while light blue or no blue indicates sites with low collagen content). Constituent proportions were determined using the ImageJ software (ImageJ; NIH, Bethesda, MD, USA) and were expressed as a percentage of the total excised lesion area. We were unable to quantify the lipid-rich (LpRi) region since such constituent did not appear clearly in lesion samples. However, the presence of macrophage-derived foam-cells and lipid crystals was analyzed. From this histological analysis performed by biologists, plaque composition was subdivided in two groups. The first group named "low collagen content" included constituents without or with few collagen (*i.e.*, thrombosis + fibrin + cellular fibrosis). The second group included constituents with high collagen content (*i.e.*, hypocellular fibrosis + collagen). Then, both low and high collagen areas were expressed as a percentage of the total excised lesion area.

Correlation between lesion contents and plaque stiffness

Based on the study of (Lee et al. 1991) conducted on mechanical properties of human atherosclerotic plaques, two groups of stiffness were defined. The soft medium consisted of plaque regions with Young's moduli ranging between 5 kPa and 700 kPa, and the stiff medium was defined as lesion sites with Young's moduli >700 kPa. These areas were expressed as a percentage of the total excised lesion area. Correlations between these two families with distinct rigidities (determined from computed modulograms) and plaque composition (obtained by histology) were analyzed using a commercially available software package (SigmaStat 3.5; Systat Software, Point Richmond, CA, USA). Regressions with p values of <0.05 were considered statistically significant. Since the plaque was partially removed during DCA intervention, the comparison study was conducted on a specific region of each modulogram which was roughly defined by the cardiologist on the pre DCA IVUS image. This approach allowed us to define the specific modulogram's region that was correlated with the histologic measurements of the excised lesion.

Table 1. Number of computed displacement fields, RF-correlation coefficient maps, strain fields and modulograms at each step of the iterative four-criterion selection procedure

		Number of frames with satisfactory							
		Displacement field		RF-correlation map		Strain field		Modulogram	
		Criteria thresholds		Criteria thresholds		Criteria thresholds		Criteria thresholds	
Patient #	Number of recorded frames	50%	60%	50%	60%	50%	60%	50%	60%
1	28	27	26	27	26	2	0	2	0
2	28	28	28	28	28	25	22	3	3
3	27	23	15	23	10	3	0	3	0
4	29	27	25	27	21	2	0	2	0
5	29	28	28	28	28	20	11	3	3
6	28	28	28	28	28	2	0	2	0
7	27	1	1	1	1	0	0	0	0
8	28	27	27	27	27	8	1	3	1
9	29	14	13	14	13	9	4	3	3
10	29	28	28	28	28	20	14	3	3
11	28	28	24	28	23	8	5	3	3
12	27	24	22	24	21	11	4	3	2
Total	337	283	265	283	254	110	61	30	18

Simulations were performed with two criteria thresholds (namely 50% and 60%). The four criteria Q_{displa}, Q_{track}, Q_{strain} and Q_{reprod} were used to extract accurate modulograms with regard to the quality of the displacement, RF-correlation coefficient, strain and reproducible elasticity maps, respectively.

RESULTS

Performance of the four-criterion selection procedure (4-CSP)

A total of 337 measured displacement, RF-correlation coefficient and measured strain maps and 254 computed strain and modulograms were computed. Table 1 provides details for each analyzed plaque, regarding the number of computed displacement fields, RF-correlation coefficient maps, strain fields and modulograms at each step of the iterative 4-CSP. Using this procedure, we could select at least one modulogram over all available frames for seven of the 12 patients (*i.e.*, for 58% of the population). For one of these seven patients (patient 8), only one modulogram fulfilling the 4-CSP was obtained while more than two reproducible modulograms were computed for the six other patients.

Performance of the plaque elasticity reconstruction algorithm

Figure 2 displays the best computed modulogram and the associated displacement, RF-correlation coefficient and radial strain (measured ε_{rr}^{LSME} and computed ε_{rr}^{iMOD}) maps obtained for patient 9. The modulogram reveals an extensive endoluminal soft region between 8 and 12 o'clock (mean Young's modulus <25 kPa). This soft region correlates well to the high strain site and corresponds to a region with almost no tissue overlap and with high values of the local RF-correlation coefficients. Figure 3 presents modulograms computed for plaques of patients 8, 11 and 12. The strong similarities found between the computed and measured strain fields (in both Figs. 2

and 3) point out the performance of the Young's modulus reconstruction technique combined with the 4-CSP.

Reproducible modulograms within a cardiac cycle

In five patients (patients 2, 5, 9, 10 and 11, Table 1), we successfully extracted three reproducible modulograms from the IVUS scan of the one cardiac cycle available. Illustrations of such sets of reproducible modulograms for patients 2 and 10 are presented in Figures 4 and 5, respectively. The data revealed that approximately two-thirds of selected modulograms were computed during the decrease of the coronary pressure.

Severity of each individual criterion

Plaque elasticity reconstructions were also conducted by considering one-criterion selection procedure (1-CSP) at a time (*i.e.*, either Q_{displa}, Q_{track}, Q_{strain} or Q_{reprod}). A quality index threshold of 60% was also selected for these computations. The most selective criterion was the strain quality index Q_{strain} since the plaque elasticity reconstruction was possible for only 20% of the total number of frames. The other indexes Q_{displa}, Q_{track} and Q_{reprod} were less restrictive since modulograms could be reconstructed for 79%, 77% and 70% of total frames, respectively (Fig. 6).

Importance of the threshold value for the 4-CSP

Interestingly, by reducing the threshold values of the four quality indexes Q_{displa}, Q_{track}, Q_{strain} and Q_{reprod} to 50%, we found more than two reproducible modulograms for 11 of the 12 patients (*i.e.*, for 92% of the population, see Table 1).
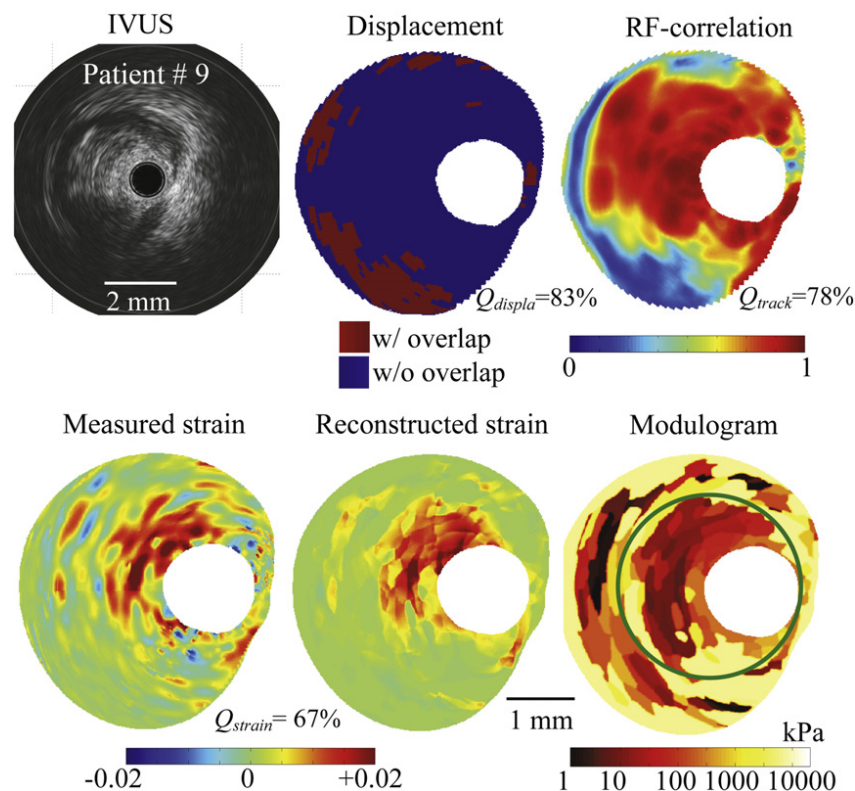
Fig. 2. Performance of the four-criterion selection procedure to extract morphology and elasticity map from the intravascular ultrasound (IVUS) sequence of patient 9. Notice that regions with tissue overlap, observed in the displacement map, correlate well with low RF-correlation coefficient sites. The high value of the strain quality index found ($Q_{strain} = 67\%$) indicates that the method reproduced reasonably the measured radial strain field. The green contour in the modulogram corresponds to the boundary of the lesion that was excised during the directional coronary atherectomy (DCA) procedure.

Histologic study of the excised plaque samples

Histologic analysis was performed on the stained samples of the seven excised lesions for which modulograms could be obtained (Fig. 7). All lesions were found with significant densities of cellular fibrosis (CeFb), collagen (Co) and fibrin (Fi) (mean values: $37.5\% \pm 21.7\%$, $25.3\% \pm 17.5\%$ and $22.2\% \pm 16.2\%$ of the total excised lesion area, respectively). Few hypocellular fibrosis (HyFb) and thrombosis (Thb) were found (mean values: $10.4\% \pm 10.7\%$ and $4.6\% \pm 5.9\%$, respectively). Foam-cells and lipid crystals were present in 7/7 and 6/7 samples, respectively. Table 2 summarizes our findings.

Correlation between excised lesion content and tissue stiffness

A strong correlation ($p < 0.035$ and $R = 0.79$) was found between the percentage of plaque area of distinct stiffness (namely [5–700 kPa] and >700 kPa, derived from computed modulograms) and the percentage of plaque area with low collagen content (*i.e.*, cellular fibrosis + thrombosis + fibrin) and high collagen content (*i.e.*, hypocellular fibrosis + collagen) obtained from the

histologic analysis, respectively (Fig. 8). Moreover, since stiffness range and plaque composition were divided into two groups, a similar correlation was found between the percentage of stiff plaque area (stiffness >700 kPa, derived from the computed modulograms) and the percentage of plaque area with high collagen content (*i.e.*, hypocellular fibrosis + collagen).

DISCUSSION

A critical key in prediction of plaque rupture is the accurate quantification of both the morphology and mechanical properties of the diseased artery (Cheng et al. 1993; Finet et al. 2004). Whereas several theories were developed to reconstruct the plaque elasticity map based on the strain field measurement (Doyley 2012), none of them preconditioned the algorithm by selecting reliable input strain and displacement fields to prevent several sources of artifacts that can be encountered *in vivo*. Therefore, in this work, we designed a four-criterion selection procedure for this purpose.

Our data demonstrate that performing the 4-CSP procedure is an essential step to obtain *in vivo* coronary
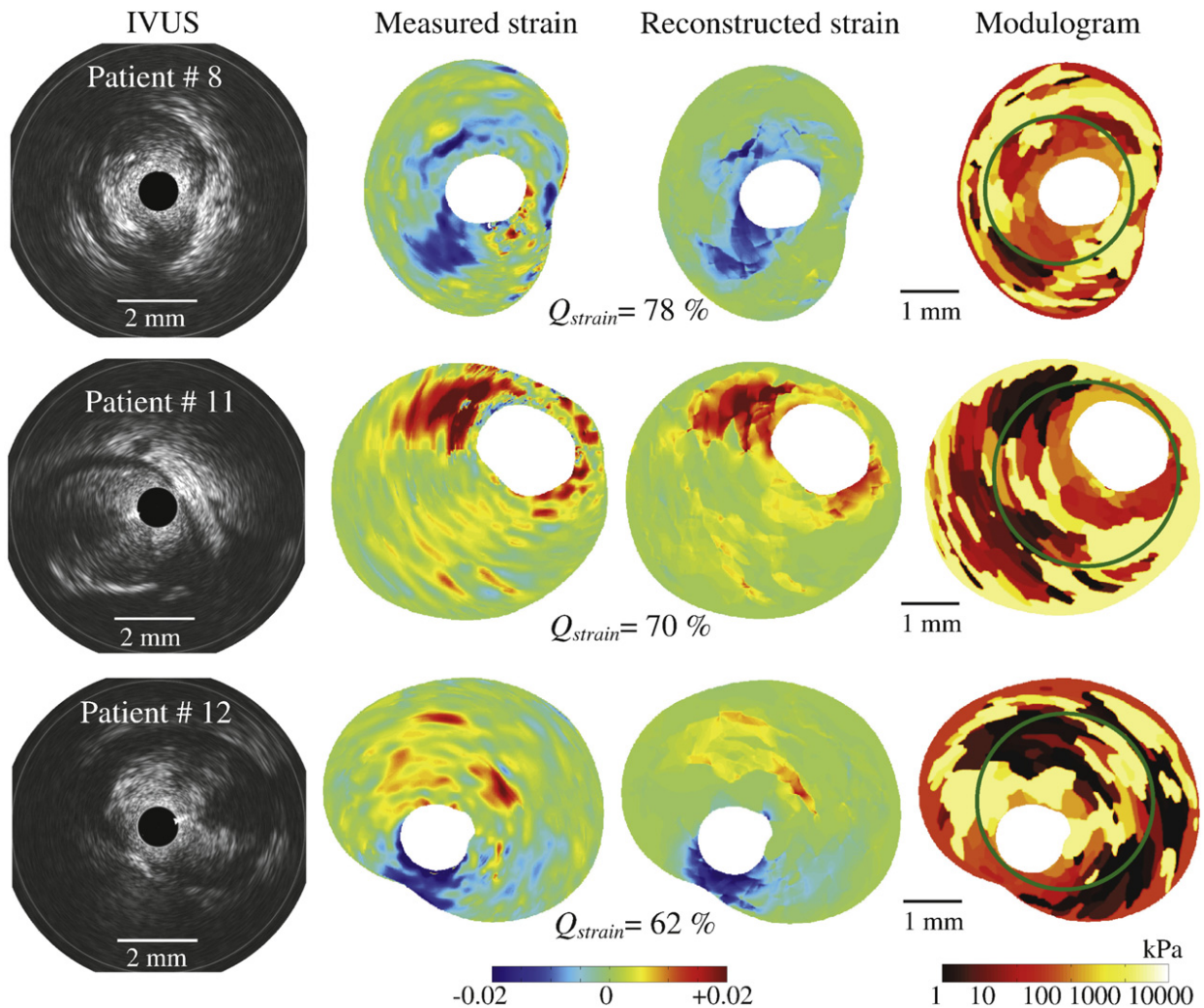
Fig. 3. Performance of the four-criterion selection procedure to extract morphologies and elasticity maps from IVUS sequences of patients 8, 11 and 12. Plaques of patients 11 and 12 have large necrotic cores (dark regions in the modulograms). The vulnerable plaque of patient 8 appears to be likely stable since the small necrotic core at 7 o'clock is far from the lumen. The green contours in the modulograms correspond to the boundaries of the lesions that were excised during the directional coronary atherectomy (DCA) procedure.

IVUS strain sequences using reconstructed elasticity methods. The results showed strong correlations between the computed and the measured radial strain fields and between plaque constituents and Young's modulus amplitudes. Moreover, the reproducibility of the computed modulograms highlighted the robustness of the 4-CSP to extract accurate elasticity maps.

Is the 4-CSP sufficient for an accurate plaque elasticity reconstruction?

Due to the motion of the heart, frames acquired at the different blood pressures may be misaligned preventing optimum strain field measurements and precise tracking of a same vessel cross-section during the whole cardiac cycle. Therefore, in their IVUS strain elastography study, de Korte et al. (2000) used a similarity index between sequential echo frames which excludes such misaligned frames. We did not used the similarity index proposed by de Korte since our 4-CSP was already able to detect such misaligned frames. Indeed, our tracking quality index Q_{track} allowed excluding frames that were poorly tracked due to the out of plane motion of the catheter.

As suggested by a few authors (Li et al. 2008; Sumi 2008), the local RF-correlation coefficient q_{correl} and the displacement index q_{displa} can be used to increase the performance of the optimization scheme. Indeed, since our methodology allowed clearly identifying plaque sites with tissue overlaps and poor correlation coefficients, it is legitimate to disregard such locations from the optimization process for an optimum elasticity map reconstruction. To investigate this point, we modified the initial RMS_{error} cost function
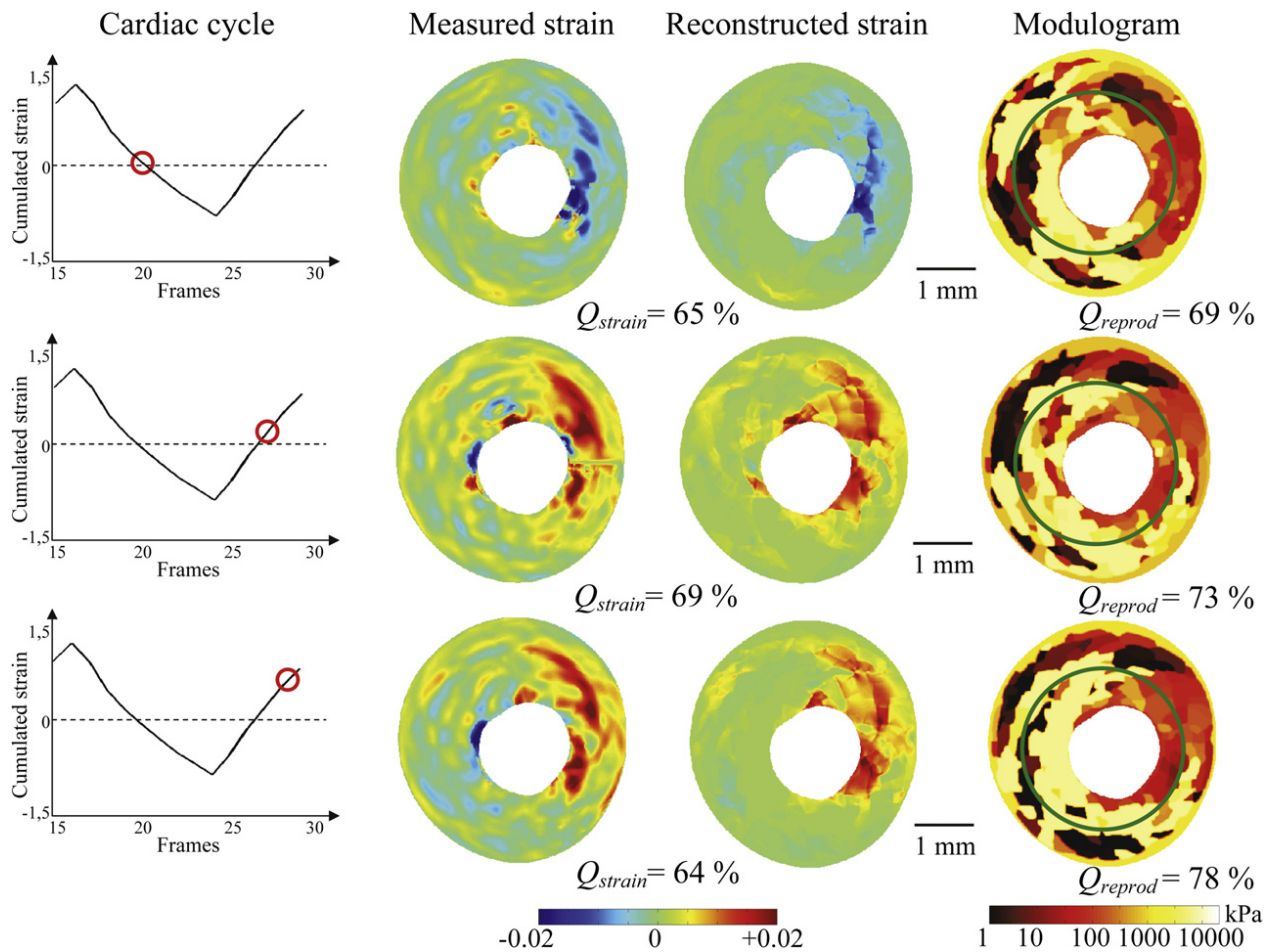
Fig. 4. Performance of the four-criterion selection procedure to extract reproducible modulograms from the intravascular ultrasound (IVUS) sequence of patient 10. Approximately two-thirds of the computed modulograms were obtained during the decrease of the coronary blood pressure (corresponding to an increase of the cumulated radial strain). The green contours in the modulograms correspond to the boundaries of the lesion that was excised during the directional coronary atherectomy (DCA) procedure.

given by eqn (1), by including the local RF-correlation coefficient q_{correl} as a weighting term:

$$RMS^*_{error}(t_j) = \frac{1}{n^*} \sqrt{\sum_{i=1}^{n^*} q_{correl}(t_j, x_i) q_{displa}(t_j, x_i) \left[\varepsilon_{rr}^{LSME}(t_j, x_i) - \varepsilon_{rr}^{iMOD}(t_j, x_i) \right]^2} \tag{7}$$

where n* is the total number of nodes in the plaque mesh excluding overlap sites (i.e. sites where $q_{displa} = 0$). For each patient, we investigated the performance of this alternative cost function RMS^*_{error} by considering only frames for which the quality indexes Q_{displa}, Q_{track} and Q_{strain} were above 60%. Interestingly, the modulograms computed with the modified cost function (eqn [7]) were found similar

to those computed with the initial cost function (eqn [1]) since the mean reproducibility index was found larger than 90% (Fig. 9). This result confirms the stability of the proposed method. Moreover, Doyley (2012) in his elegant review article mentioned the uniqueness of the mathematical solution for such hard-prior elasticity reconstruction method, which does not require any type of regularization since the reconstruction problem is well conditioned. However, such technique is prone to errors because the
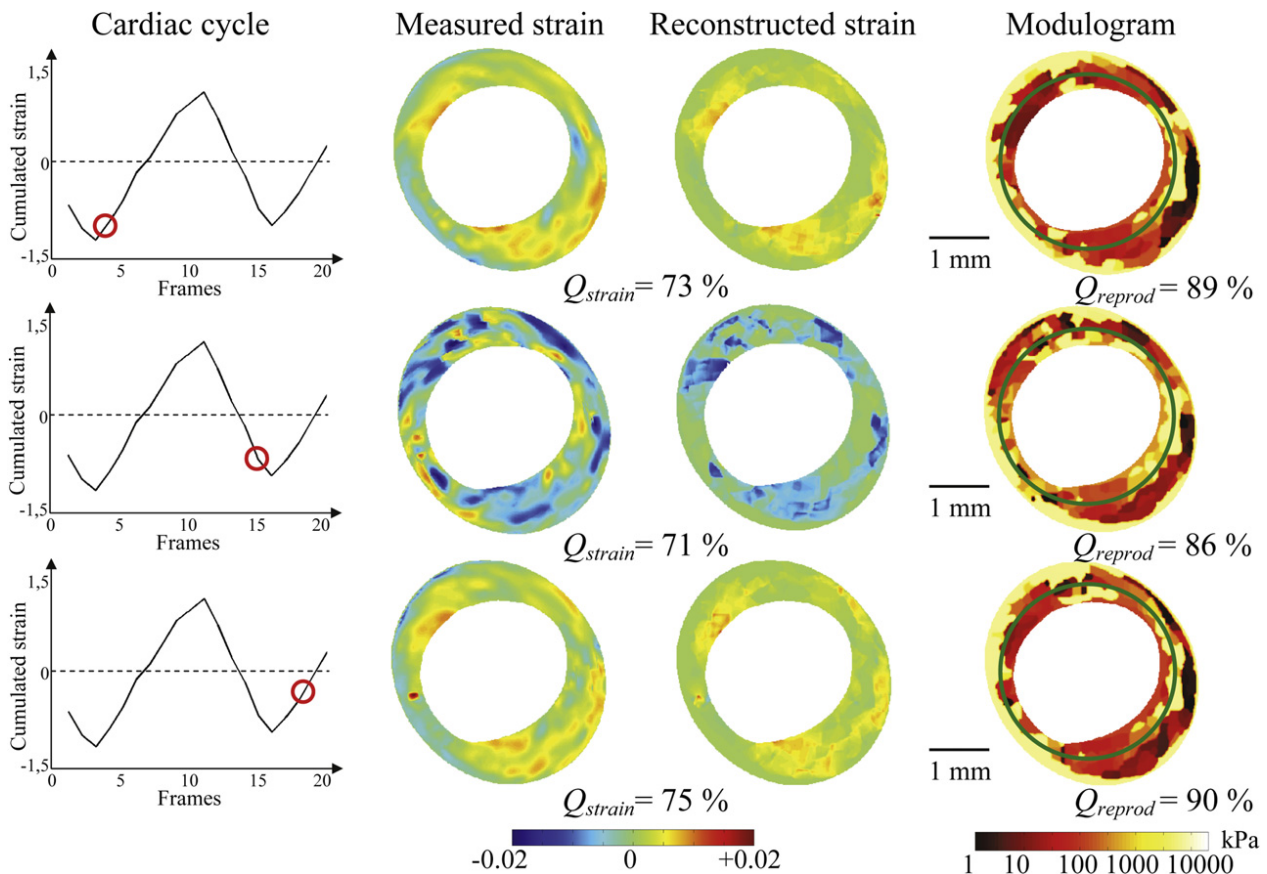
Fig. 5. Performance of the four-criterion selection procedure to extract reproducible modulograms from the intravascular ultrasound (IVUS) sequence of patient 2. The strong correlations found between the computed and the measured radial strain fields ($Q_{strain} > 70\%$) and the significant reproducibility of the three resulting modulograms highlight the robustness of the method. The green contours in the modulograms correspond to the boundaries of the lesion that was excised during the directional coronary atherectomy (DCA) procedure.

DWS preconditioning step may generate some errors during the segmentation procedure (Doyley 2012).

What is the most appropriate cardiac phase to estimate modulograms?

Baldewsing and coworkers (2008) observed that the decrease of the arterial pressure was a more appropriate cardiac phase to extract reliable strain fields during *in vivo* IVUS sequence of a vulnerable plaque. Our results are in agreement, as 66% of our extracted reliable modulograms were obtained during the decrease of the coronary blood pressure.

Is the elastogram sufficient to detect vulnerable plaques?

Knowing that the rate of deformation (strain) of a tissue is directly related to the stress applied on it and to its mechanical properties, Ophir and colleagues (Ophir et al. 1991; Cespedes et al. 1993) were the pioneers on developing imaging techniques based on the strain field. In this context, several elegant IVUS strain reconstructions (de Korte et al. 2002; Maurice

et al. 2007) and palpography methods (Schaar et al. 2003) were developed to investigate atherosclerotic coronary artery plaques and to predict their vulnerability to
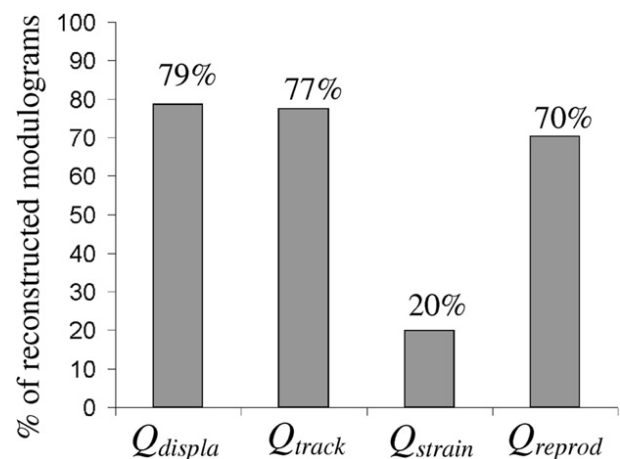

Fig. 6. Results regarding the severity of each criterion. The strain quality index Q_{strain} was found to be the most selective since modulograms were reconstructed for 20% of the total recorded frames only.
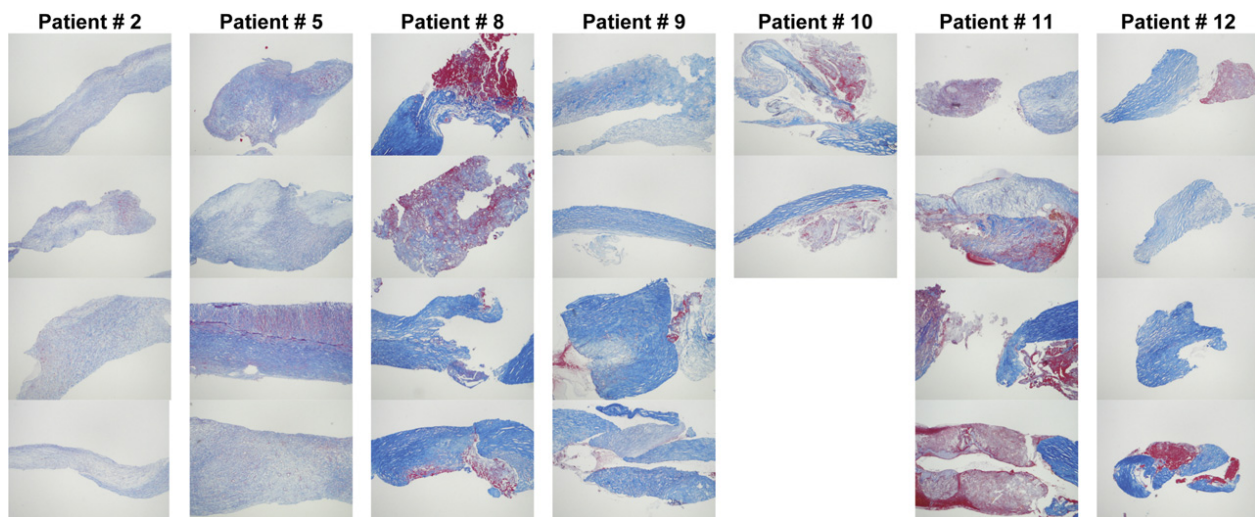
Fig. 7. Microscopic images of the histologic stained samples of the seven excised lesions for which modulograms were obtained. The elastica-Masson's trichrome (EMT) staining was used to characterize the composition of the atherosclerotic excised lesions. These stained samples were used for the histologic study.

rupture. Techniques based on the optical flow (Maurice et al. 2004) or time-delay correlation estimation (de Korte et al. 2002) allowed the calculations of intraplaque strain images during the cardiac cycle. Their main approach to detect VP was based on the idea that the deformation of soft plaque heterogeneities (*i.e.*, the lipid core) should be much larger than those of stiff inclusions (*i.e.*, calcified and fibrosis areas) in response to blood pressure changes (de Korte et al. 2002). However, these methods did not overcome a main limitation (de Korte et al. 2007) related to the complex geometries of atherosclerotic plaques, which alter the intraplaque strain fields and inhibit direct translation into Young's modulus maps. Figure 3 indeed demonstrates clearly such limitation. The strain map of patient 8 (Fig. 3) highlights a high strain site located at the endoluminal layer between 6 and 8 o'clock. The strain field alone seems to indicate that the plaque is vulnerable and unstable with the possibility of a large necrotic core close to the lumen. However, the associated modulogram reveals a small soft region in the deeper plaque layer with a thick and stiff fibrous cap (cap thickness >800 μm and mean Young's modulus close to 335 kPa).

Study limitations

Several limitations deserve to be pointed out, even if the results include findings which may help to increase the performance of the modulography technique:

First, despite our elasticity reconstruction maps being based on real *in vivo* IVUS data, correlations between patient's modulogram and the histological analysis of the associated excised lesion presented in this study were relevant, but not sufficient to broadly validate our computational findings. However, our findings are supported by a preclinical study showing that the plaque morphology and mechanical properties of the atherosclerotic lesion can be accurately derived by using the proposed modulography approach (Le Floc'h et al. 2010).

Second, an important study limitation remains the assumption made on blood pressure. Indeed, since blood pressure was not measured during the IVUS acquisition sequence, the modulograms were obtained by assuming a bilinear pressure-time evolution during cardiac cycle. Such assumption may bias the resulting modulogram. However, by using a linear elasticity theory to solve the

Table 2. Histologic measurements

Patient #	Thb (%)	Fi (%)	CeFb (%)	HyFb (%)	Co (%)
2	0	5	63	32	0
5	0	15	68	3	14
8	9	34	26	2	29
9	0	9	45	7	39
10	0	43	16	15	26
11	14	40	18	12	16
12	9	10	25	3	53
Mean ± SD	4.6 ± 5.9	22.2 ± 16.2	37.5 ± 21.7	10.4 ± 10.7	25.3 ± 17.5

Thb = thrombosis; Fi = Fibrin; CeFb = cellular fibrosis; HyFb = hypocellular fibrosis; Co = collagen.
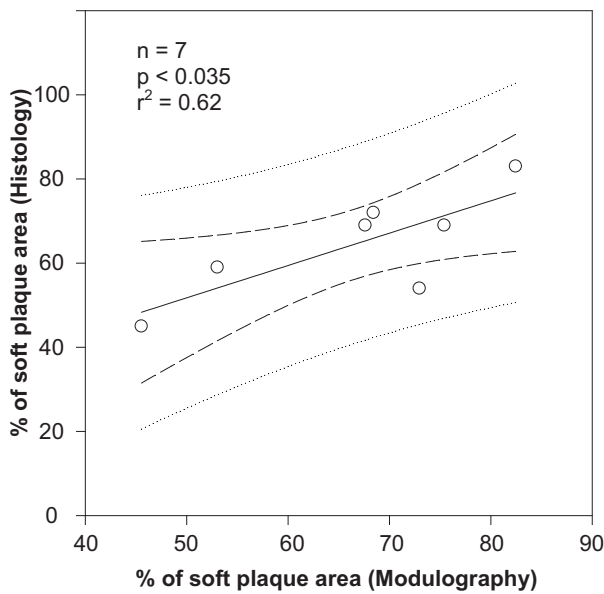Excised lesions composition, expressed as percent of total plaque area.

Fig. 8. A good agreement was found when comparing the percentage of soft plaque area (*i.e.*, 5 kPa <stiffness <700 kPa) values derived from the computed modulograms with the percentage of plaque area with low collagen content (*i.e.*, cellular fibrosis + thrombosis + fibrin) obtained from the histological analysis. The linear regression line (dark line) and the confidence of the prediction interval domains, which are the domain limited by the two internal and external dashed lines, respectively, are also given.

inverse problem, the values of the Young's modulus solutions appear to be proportional to the pressure gradient amplitude. Therefore, one option to overcome such limitation, would have been to normalize the Young's modulus by the pressure gradient amplitude to obtain

a normalized modulogram. Such option was not chosen since the mean relative error made by assuming such simplified linear temporal pressure distribution was found lower than 26% (results not shown). We quantified such error by comparing the pressure gradient amplitude obtained with the bilinear curve with the one obtained by considering a more realistic pressure-time curve.

Third, the proposed technique for rigid motion compensation between consecutive frames does not correct for the non uniform rotation of the single ultrasound probe element that may affect the resulting strain elastogram.

Finally, the influence of residual stresses (Matsumoto et al. 2004), generated by remodeling and plaque growth processes, have been ignored in this study. Residual stress patterns have been studied *ex vivo* in several human vulnerable coronary plaque samples (Ohayon et al. 2007). Neglecting residual stresses in structural analysis could bias the mechanical stress quantification but not the characterization of the mechanical properties, which was the main goal of this study.

Clinical implications

Increased arterial stiffness is associated with markers of cardiovascular risk (Glasser et al. 1997; Van Bortel et al. 2001). Our group recently showed that local increase of vessel stiffness resulting from wall-strain stiffening phenomenon is critical in the evolution of atherosclerotic lesions (Ohayon et al. 2011). The proposed LSME-iMOD imaging method may help in localizing such sensitive zones.

Several animal and clinical studies conducted to analyze the structural variation in the fibrous cap and necrotic core demonstrated that statin treatment enhances
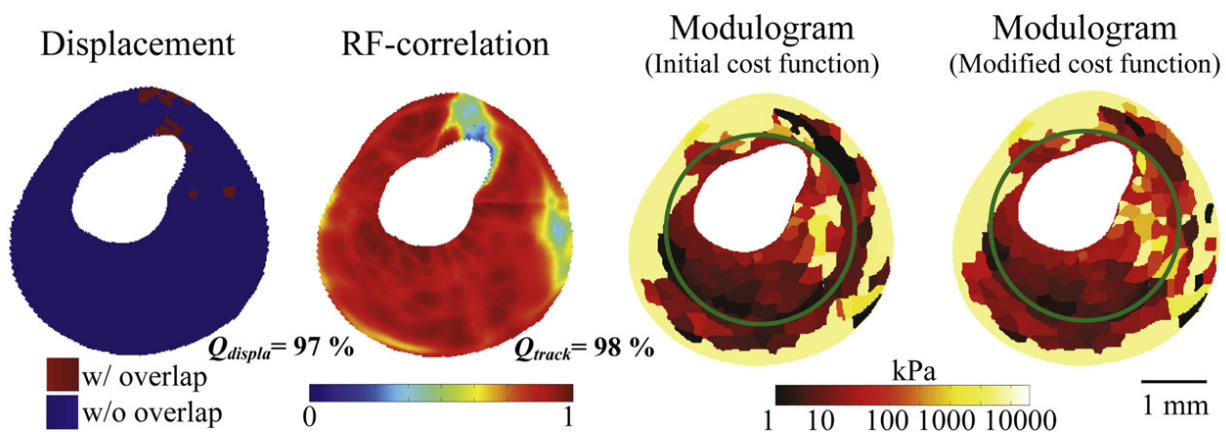

Fig. 9. Performance of the considered cost function (see eqn [1]) in the optimization algorithm. Improving the cost function (see eqn [7]) by restricting the optimization process to only regions with no tissue overlap and with high RF-correlation coefficients did not modify significantly the resulting modulograms. These simulations were performed on patient 5. This result demonstrates the stability and robustness of the proposed four-criterion selection procedure. The green contours in the modulograms correspond to the boundaries of the lesion that was excised during the directional coronary atherectomy (DCA) procedure.

plaque stability (Libby et al. 2002). Furthermore, as suggested in a previous study (Finet et al. 2004), a very slight increase in the mechanical properties of plaque constituents, namely the hardening of the necrotic core, can tilt a VP from instability to stability. The proposed LSME-iMOD imaging method may be used to explain such findings (Nozue et al. 2012) by investigating the evolution of mechanical properties of atherosclerotic plaques during the statin therapy.

REFERENCES

Arroyo LH, Lee RT. Mechanisms of plaque rupture: Mechanical and biologic interactions. Cardiovasc Res 1999;41:369–375.

Arts T, Prinzen FW, Delhaas T, Milles JR, Rossi AC, Claryssee P. Mapping displacement and deformation of the heart with local sine-wave modeling. IEEE Trans Med Imaging 2010;29: 1114–1123.

Baldewsing RA, Danilouchkine MG, Mastik F, Schaar JA, Serruys PW, van der Steen AF. An inverse method for imaging the local elasticity of atherosclerotic coronary plaques. IEEE Trans Inf Technol Biomed 2008;12:277–289.

Beattie D, Xu C, Vito R, Glagov S, Whang MC. Mechanical analysis of heterogeneous, atherosclerotic human aorta. J Biomech Eng 1998; 120:602–607.

Briley-Saebo KC, Mulder WJ, Mani V, Hyafil F, Amirbekian V, Aguinaldo JG, Fisher EA, Fayad ZA. Magnetic resonance imaging of vulnerable atherosclerotic plaques: Current imaging strategies and molecular imaging probes. J Magn Reson Imaging 2007;26: 460–479.

Carlier SG, Tanaka K. Studying coronary plaque regression with IVUS: A critical review of recent studies. J Interv Cardiol 2006;19:11–15.

Cespedes I, Ophir J, Ponnekanti H, Maklad N. Elastography: Elasticity imaging using ultrasound with application to muscle and breast *in vivo*. Ultrason Imaging 1993;15:73–88.

Chan RC. OCT-based arterial elastography: Robust estimation exploiting tissue biomechanics. Optics Express 2004;12:4558–4572.

Cheng GC, Loree HM, Kamm RD, Fishbein MC, Lee RT. Distribution of circumferential stress in ruptured and stable atherosclerotic lesions. A structural analysis with histopathological correlation. Circulation 1993;87:1179–1187.

Cimrman R, Rohan E. On the identification of the arterial model parameters from experiments applicable "*in vivo*". Math Comput Simulation 2010;80:1232–1245.

de Korte CL, van der Steen AFW, Céspedes EI, Pasterkamp G, Carlier SG, Mastik F, Schoneveld AH, Serruys PW, Bom N. Characterization of plaque components and vulnerability with intravascular ultrasound elastography. Phys Med Biol 2000;45:1465–1475.

de Korte CL, Carlier SG, Mastik F, Doyley MM, van der Steen AF, Serruys PW, Bom N. Morphological and mechanical information of coronary arteries obtained with intravascular elastography; feasibility study *in vivo*. Eur Heart J 2002;23:405–413.

de Korte CL, Mastik F, De Feyter PJ, Slager CL, Van der Steen AF, Serruys PW. Intravascular palpography. In: Virmani R, Narula J, Leon MB, Willerson JT, (eds). The vulnerable atherosclerotic plaque: Strategies for diagnosis and management. Malden, MA: Blackwell Futura 2007:289–296.

Doyley MM. Model-based elastography: A survey of approaches to the inverse elasticity problem. Phys Med Biol 2012;57:R35–R73.

Falk E, Shah PK, Fuster V. Coronary plaque disruption. Circulation 1995;92:657–671.

Fehrenbach J, Masmoudi M, Souchon R, Trompette P. Detection of small inclusions by elastography. Inverse Problems 2006;22:1055.

Finet G, Ohayon J, Rioufol G. Biomechanical interaction between cap thickness, lipid core composition and blood pressure in vulnerable coronary plaque: Impact on stability or instability. Coron Artery Dis 2004;15:13–20.

Franquet A, Avril S, Le Riche R, Badel P. Identification of heterogeneous elastic properties in stenosed arteries: A numerical plane strain study. Comput Methods Biomech Biomed Engin 2012;15: 49–58.

Glasser SP, Arnett DK, McVeigh GE, Finkelstein SM, Bank AJ, Morgan DJ, Cohn JN. Vascular compliance and cardiovascular disease: A risk factor or a marker? Am J Hypertens 1997;10: 1175–1189.

Hu XB, Zhang PF, Su HJ, Yi X, Chen L, Rong YY, Zhang K, Li X, Wang L, Sun CL, Cai XJ, Li L, Song JT, Dai XM, Sui XD, Zhang Y, Zhang M. Intravascular ultrasound area strain imaging used to characterize tissue components and assess vulnerability of atherosclerotic plaques in a rabbit model. Ultrasound Med Biol 2011;37:1579–1587.

Jang IK, Bouma BE, Kang DH, Park SJ, Park SW, Seung KB, Choi KB, Shishkov M, Schlendorf K, Pomerantsev E, Houser SL, Aretz HT, Tearney GJ. Visualization of coronary atherosclerotic plaques in patients using optical coherence tomography: Comparison with intravascular ultrasound. J Am Coll Cardiol 2002;39:604–609.

Kim K, Weitzel WF, Rubin JM, Xie H, Chen X, O'Donnell M. Vascular intramural strain imaging using arterial pressure equalization. Ultrasound Med Biol 2004;30:761–771.

Larose E, Yeghiazarians Y, Libby P, Yucel EK, Aikawa M, Kacher DF, Aikawa E, Kinlay S, Schoen FJ, Selwyn AP, Ganz P. Characterization of human atherosclerotic plaques by intravascular magnetic resonance imaging. Circulation 2005;112:2324–2331.

Le Floc'h S, Cloutier G, Finet G, Tracqui P, Pettigrew RI, Ohayon J. On the potential of a new IVUS elasticity modulus imaging approach for detecting vulnerable atherosclerotic coronary plaques: *In vitro* vessel phantom study. Phys Med Biol 2010;55:5701–5721.

Le Floc'h S, Ohayon J, Tracqui P, Finet G, Gharib AM, Maurice RL, Cloutier G, Pettigrew RI. Vulnerable atherosclerotic plaque elasticity reconstruction based on a segmentation-driven optimization procedure using strain measurements: Theoretical framework. IEEE Trans Med Imaging 2009;28:1126–1137.

Lee RT, Grodzinsky AJ, Frank EH, Kamm RD, Schoen FJ. Structure-dependent dynamic mechanical behavior of fibrous caps from human atherosclerotic plaques. Circulation 1991;83:1764–1770.

Li J, Cui Y, Kadour M, Noble JA. Elasticity reconstruction from displacement and confidence measures of a multi-compressed ultrasound RF sequence. IEEE Trans Ultrason Ferroelectr Freq Control 2008;55:319–326.

Libby P, Ridker PM, Maseri A. Inflammation and atherosclerosis. Circulation 2002;105:1135–1143.

Loree HM, Kamm RD, Stringfellow RG, Lee RT. Effects of fibrous cap thickness on peak circumferential stress in model atherosclerotic vessels. Circ Res 1992;71:850–858.

Matsumoto T, Goto T, Furukawa T, Sato M. Residual stress and strain in the lamellar unit of the porcine aorta: Experiment and analysis. J Biomech 2004;37:807–815.

Maurice RL, Fromageau J, Brusseau E, Finet G, Rioufol G, Cloutier G. On the potential of the lagrangian estimator for endovascular

ultrasound elastography: *In vivo* human coronary artery study. Ultrasound Med Biol 2007;33:1199–1205.

Maurice RL, Ohayon J, Finet G, Cloutier G. Adapting the Lagrangian speckle model estimator for endovascular elastography: Theory and validation with simulated radio-frequency data. J Acoust Soc Am 2004;116:1276–1286.

Nozue T, Yamamoto S, Tohyama S, Umezawa S, Kunishima T, Sato A, Miyake S, Takeyama Y, Morino Y, Yamauchi T, Muramatsu T, Hibi K, Sozu T, Terashima M, Michishita I. Statin treatment for coronary artery plaque composition based on intravascular ultrasound radiofrequency data analysis. Am Heart J 2012;163: 191–199 e1.

Ohayon J, Dubreuil O, Tracqui P, Le Floc'h S, Rioufol G, Chalabreysse L, Thivolet F, Pettigrew RI, Finet G. Influence of residual stress/strain on the biomechanical stability of vulnerable coronary plaques: Potential impact for evaluating the risk of plaque rupture. Am J Physiol Heart Circ Physiol 2007;293:H1987–H1996.

Ohayon J, Finet G, Gharib AM, Herzka DA, Tracqui P, Heroux J, Rioufol G, Kotys MS, Elagha A, Pettigrew RI. Necrotic core thickness and positive arterial remodeling index: Emergent biomechanical factors for evaluating the risk of plaque rupture. Am J Physiol Heart Circ Physiol 2008;295:H717–H727.

Ohayon J, Gharib AM, Garcia A, Heroux J, Yazdani SK, Malve M, Tracqui P, Martinez MA, Doblare M, Finet G, Pettigrew RI. Is arterial wall-strain stiffening an additional process responsible for atherosclerosis in coronary bifurcations? An *in vivo* study based on dynamic CT and MRI. Am J Physiol Heart Circ Physiol 2011; 301:H1097–H1106.

Ohayon J, Teppaz P, Finet G, Rioufol G. In-vivo prediction of human coronary plaque rupture location using intravascular ultrasound and the finite element method. Coron Artery Dis 2001;12:655–663.

Ophir J, Cespedes I, Ponnekanti H, Yazdi Y, Li X. Elastography: A quantitative method for imaging the elasticity of biological tissues. Ultrason Imaging 1991;13:111–134.

Pazos V, Mongrain R, Tardif JC. Mechanical characterization of atherosclerotic arteries using finite element modeling: Feasibility study on mock arteries. IEEE Trans Biomed Eng 2010;57:1520–1528.

Richards MS, Doyley MM. Investigating the impact of spatial priors on the performance of model-based IVUS elastography. Phys Med Biol 2011;56:7223–7246.

Rioufol G, Finet G, Ginon I, Andre-Fouet X, Rossi R, Vialle E, Desjoyaux E, Convert G, Huret JF, Tabib A. Multiple atherosclerotic plaque rupture in acute coronary syndrome: A three-vessel intravascular ultrasound study. Circulation 2002;106:804–808.

Rogowska J, Patel NA, Fujimoto JG, Brezinski ME. Optical coherence tomographic elastography technique for measuring deformation and strain of atherosclerotic tissues. Heart 2004;90:556–562.

Roy Cardinal MH, Meunier J, Soulez G, Maurice RL, Therasse E, Cloutier G. Intravascular ultrasound image segmentation: A three-dimensional fast-marching method based on gray level distributions. IEEE Trans Med Imaging 2006;25:590–601.

Schaar JA, de Korte CL, Mastik F, Baldewsing R, Regar E, de Feyter P, Slager CJ, van der Steen AF, Serruys PW. Intravascular palpography for high-risk vulnerable plaque assessment. Herz 2003;28:488–495.

Sumi C. Regularization of tissue shear modulus reconstruction using strain variance. IEEE Trans Ultrason Ferroelectr Freq Control 2008;55:297–307.

Tearney GJ, Waxman S, Shishkov M, Vakoc BJ, Suter MJ, Freilich MI, Desjardins AE, Oh WY, Bartlett LA, Rosenberg M, Bouma BE. Three-dimensional coronary artery microscopy by intracoronary optical frequency domain imaging. JACC Cardiovasc Imaging 2008;1:752–761.

Van Bortel LM, Struijker-Boudier HA, Safar ME. Pulse pressure, arterial stiffness, and drug treatment of hypertension. Hypertension 2001;38:914–921.

van Soest G, Mastik F, de Jong N, van der Steen AF. Robust intravascular optical coherence elastography by line correlations. Phys Med Biol 2007;52:2445–2458.

Virmani R, Burke AP, Farb A, Kolodgie FD. Pathology of the vulnerable plaque. J Am Coll Cardiol 2006;47:C13–C18.

Virmani R, Kolodgie FD, Burke AP, Farb A, Schwartz SM. Lessons from sudden coronary death: A comprehensive morphological classification scheme for atherosclerotic lesions. Arterioscler Thromb Vasc Biol 2000;20:1262–1275.

Vonesh MJ, Cho CH, Pinto JV Jr, Kane BJ, Lee DS, Roth SI, Chandran KB, McPherson DD. Regional vascular mechanical properties by 3-D intravascular ultrasound with finite-element analysis. Am J Physiol 1997;272:H425–H437.

Vorp DA, Rajagopal KR, Smolinski PJ, Borovetz HS. Identification of elastic properties of homogeneous, orthotropic vascular segments in distension. J Biomech 1995;28:501–512.

Wan M, Li Y, Li J, Cui Y, Zhou X. Strain imaging and elasticity reconstruction of arteries based on intravascular ultrasound video images. IEEE Trans Biomed Eng 2001;48:116–120.

Zhang Q, Wang Y, Wang W, Ma J, Qian J, Ge J. Automatic segmentation of calcifications in intravascular ultrasound images using snakes and the contourlet transform. Ultrasound Med Biol 2010;36: 111–129.